A model of the two-stage Hall thruster discharge

E. Ahedo[a] and F. I. Parra
Escuela Técnica Superior de Ingenieros Aeronáuticos, Universidad Politécnica de Madrid, 28040 Madrid, Spain

(Received 2 December 2004; accepted 24 May 2005; published online 20 July 2005)

The effect of a third, active electrode placed inside the ceramic chamber of a Hall thruster is analyzed. Both electron-collecting and electron-emitting modes are considered. Significant efficiency enhancement with respect to the single-stage operation can be obtained for a good electron-emitting electrode, placed in an intermediate location of the acceleration region, and for an anode-to-electrode (inner-stage) potential significantly larger than the ionization potential. Optimum values of the electrode location and voltage are determined. The performance improvement is due to a reduction of the energy losses to the chamber walls. This is the consequence of lower Joule heating and thus lower electron temperature in the outer stage. When the ionization process is efficient already in the single-stage operation, (i) two-stage operation does not affect practically the propellant and voltage utilizations and (ii) thrust efficiency decreases when the intermediate electrode works as an electron collector. © *2005 American Institute of Physics*.
[DOI: 10.1063/1.1957129]

I. INTRODUCTION

The basic two-stage configuration of a Hall thruster consists of introducing in the annular discharge chamber an additional electrode, which is biased to an intermediate potential between the upstream anode and the external cathode. Two-stage designs date back to the early times of Hall thruster development. Early Russian prototypes are reported in the review paper of Kaufman[1] (see Refs. 29–31 therein). Most two-stage designs are based on the idea of making the ion production process more independent of the acceleration process. The advantage would be that a high-current, low-voltage stage can be used to form the ions, while simultaneously, the electron backflow can be minimized through the high-voltage accelerating stage, thereby maximizing the acceleration efficiency.[1]

Thus, a double role is assigned to the intermediate electrode: (i) to provide an additional control on the axial electric potential and (ii) to deliver part of the electron current required for the gas ionization. The amount and *sign* of the current exchanged at the third electrode depend on the physical device and the potential bias between the third electrode and the surrounding plasma. To this respect, we distinguish between two basic types of electrodes: *passive* electrodes, capable only of collecting ions and electrons, and *active* electrodes, with the added capability of emitting electrons. Clearly, passive electrodes have a more limited ability to modify the characteristics of single-stage discharges, and only active electrodes can deliver a large electron current.

Two-stage designs for stationary plasma thrusters (SPT), which have long ceramic chambers, tend to use active electrodes whereas two-stage designs for thrusters with anode layer (TAL), because of their short and metallic chambers, use passive electrodes. The strong, renewed interest on Hall thrusters over the last years has reached two-stage designs too. A recent two-stage TAL prototype is the D-80, a USA-Russia project. Experimental tests with this thruster have led to mixed conclusions. On the one hand, extensive tests made at NASA conclude that, in terms of efficiency, two-stage operation of the D-80 presents no clear advantage over the single-stage operation.[2] On the other hand, a Russian set of experiments for the same thruster and constant anode-to-cathode (total) voltage finds that (i) the efficiency is maximized for a certain anode-to-third-electrode (inner-stage) voltage and (ii) two-stage operation is preferable only for high specific impulses.[3]

Most recent two-stage SPT designs use, as third electrode, a heatable, annular plate or wire of tungsten impregnated with a high electron-emission material (BaO, LaB_6,…). Yamagiwa and Kuriki designed a prototype with annular electrodes in the inner and outer walls, although only the outer-wall electrode could be heated externally; increments of efficiency were found for the two-stage operation but the maximum efficiency never exceeded 20%.[4] Fisch *et al.* tested the two-stage configurations and declared that efficiencies were similar to the conventional operation.[5] A prototype with an annular cathode wrapping most of the first stage, designed at Busek Co., showed no appreciable differences between the measured single-stage and two-stage performances.[6] Hofer *et al.* designed the P5-2 with an intermediate electrode located in the inner wall of the chamber. Although the electrode included a tungsten heating element to produce large electron emissions, tests were carried out without electrode heating (due to a fracture of the ceramic chamber and lack of time). It was concluded that the two-stage operation of P5-2 leads to a higher thrust at the expense of efficiency.[7]

This brief review shows that the performances of the present, two-stage designs do not meet yet the expectations deposited on them. It remains an open question whether their limited success is caused by (a) an insufficient understanding of the physics of two-stage discharges, (b) improper design

[a]Electronic mail: eduardo.ahedo@upm.es

or operation parameters, or (c) technical issues canceling out any gain derived from the two-stage operation. With respect to the first point there are very few theoretical studies of two-stage discharges. Fruchtman and Fisch,[8] using a simple one-dimensional (1D) model (of the plasma acceleration region *only*), showed that an optimal distribution of *electron-emitting* electrodes reduces the electron heating in that region and thus enhances the thrust efficiency. For a single intermediate electrode they found that the maximum efficiency gain, at the optimum location and voltage of the third electrode, is lower than 6%. In a parallel publication, Fruchtman *et al.*[9] analyzed a more complete 1D model of a two-stage discharge and showed that the efficiency can be enhanced *also* by using an *electron-collecting* electrode placed exactly at the sonic transition of the ion flow.

The main limitations of the model of Ref. 9 are (i) to consider constant electron temperature along the channel for different operation conditions; (ii) to fix the *moving* sonic transition point at the location of the third electrode; and (iii) to neglect the ion backstreaming region. In this paper we present a model that overcomes these drawbacks. It is based on the single-stage model of Ahedo *et al.*[10] and is applicable mainly to (i) thrusters with long ceramic chambers (SPT-type) and therefore, large wall energy losses and (ii) to electrodes with a large capability of exchanging electrons with the plasma discharge. Both the electron-emission and collection modes of the electrode will be discussed, but the study will focus on the more interesting one, the electron-emission mode. Beyond presenting the key physics governing each stage of the discharge, we carry out an extensive parametric study in order to determine the influence of the location and voltage of the third electrode for a given mass flow and total discharge voltage. The results of our model will show that the efficiency can be improved significantly by using an electron-emitting electrode and will suggest the appropriate location and voltage for that electrode.

In several of the experiments commented previously, two-stage designs are envisaged in connection with dual-mode operation of Hall thrusters. Indeed, certain authors propose to use two-stage operation for the high specific impulse (i.e., high-discharge voltage) mode, but to keep single-stage operation for the high thrust (i.e., moderate discharge voltage) mode. Clearly, "dual mode" and "two stage" are independent concepts. Two stages refer mainly to the thruster configuration, whereas dual mode refers to the operation conditions. In this paper we study the influence of the third-electrode parameters, but a full parametric characterization of a two-stage thruster (and, in particular, its dual-mode operation) is beyond the goals of this work.

The rest of the paper is organized as follows. In Sec. II, we present the two-stage model and the parameters that determine the plasma response. In Sec. III, we derive some analytical laws useful to evaluate the numerical solutions. In Sec. IV, we discuss the behavior of two-stage discharges and determine the influence of the location and voltage of the third electrode. Conclusions and final comments are presented in Sec. V.

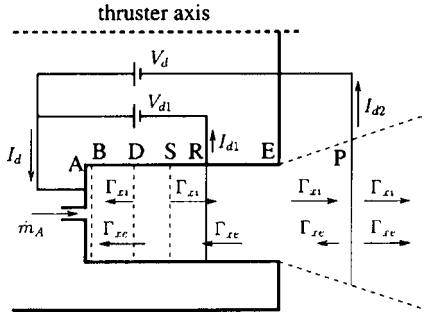

FIG. 1. Sketch of the two-stage discharge model. The anode is at point A (with $x_A=0$), the thruster exhaust at point E, the cathode neutralization surface at point P, and the third electrode at point R. The total and inner-stage discharge voltages, V_d and V_{d1}, are known, whereas the inner- and outer-stage currents, I_{d1} and I_{d2}, are part of the solution; $I_d=I_{d1}+I_{d2}$ is the total discharge current. Points D and S correspond to zero and sonic velocities of the ion flow and are obtained as part of the solution. Point B is the anode-sheath transition. Regions AB, BD, DS, SR, RP correspond to the electron-repelling sheath, ion backstreaming region, main ionization layer, inner-stage acceleration region, and outer-stage acceleration region. $\Gamma_{x\alpha}=An_\alpha v_{x\alpha}, \alpha=i,e,n$ are the axial flows of particles of each of the plasma species.

II. FORMULATION OF THE MODEL

A. Hypotheses

The two-stage model is a natural extension of the single-stage model presented in Ref. 10. A sketch of the two-stage discharge is shown in Fig. 1. The main features of the discharge model are the following:

(1) The model is stationary, macroscopic, and considers three plasma populations: ions (i), electrons (e), and neutrals (n).

(2) The average Debye length of the plasma, λ_D, is assumed to be much smaller than the typical length of the axial gradients (which usually is a fraction of the chamber length, L_c). Thus, plasma quasineutrality applies everywhere except in Debye sheaths around the chamber walls.

(3) The equations for the axial response consider plasma magnitudes that are radially averaged values of the corresponding two-dimensional (2D) variables. For instance, the r-averaged electrostatic potential is defined as

$$\phi(x)=\frac{1}{A(x)}\int_{r_{\rm in}}^{r_{\rm out}}\bar{\phi}(x,r)2\pi r dr, \tag{1}$$

with $\bar{\phi}(x,r)$ the 2D potential, and $r_{\rm in}(x), r_{\rm out}(x)$, and $A(x)$ are the inner radius, the outer radius, and the radial area of the plasma jet, respectively.

(4) The magnetic field for the 1D, axial response is assumed of the form $\boldsymbol{B}=B_r(x)\mathbf{1}_r$,. This magnetic field must be considered as an r-averaged field for the 1D model, where 2D features (such as the x-component of the field or the dependence on r) are ignored out of necessity.

(5) In addition to collisions with heavy species and wall collisionality, the electron diffusive motion is affected by turbulent (i.e., anomalous or Bohm-like) diffusion. We define the anomalous diffusion frequency as $\nu_{\rm ano}=\alpha_{\rm ano}\omega_e$, with $\omega_e=eB/m_e$ the electron gyrofrequency

and α_{ano} the relative level of the correlated azimuthal fluctuations,[10,11] which, in the absence of a satisfactory theory, is assumed constant along the channel and is adjusted by fitting the model solutions to available experimental results.

(6) The effects of the plasma interaction with the lateral walls are included in the axial equations as volumetric source terms. Their functional form are obtained from the radial model of Ahedo.[12] This considers the sheath/presheath/sheath structure between the lateral walls and takes into account the secondary-electron emission (SEE). For high SEE the charge saturation of the negative (i.e., ion attracting) sheaths prevents them from vanishing.

The specific features of the two-stage model are the following:

(1) The two-stage discharge is accomplished through an intermediate electrode placed inside the chamber. This *r*-averaged model does not distinguish whether the electrode is placed at the inner or outer wall. The electrode is treated similarly to the neutralization surface of the external cathode. The axial width of the electrode $\Delta x_{\rm int}$ is assumed to satisfy

$$\lambda_D \ll \Delta x_{\rm int} \ll L_c, \tag{2}$$

so that we can consider that the exchange of electric current at the intermediate electrode, I_{d1}, takes place at a single axial position, point R in Fig. 1. (In a 2D model this current would be delivered along the magnetic-field line intersecting the electrode).

(2) The two-stage discharge is controlled by the total discharge voltage V_d and the inner-stage voltage V_{d1}; thus, the outer-stage voltage is $V_{d2}=V_d-V_{d1}$. Although it is electrically equivalent to operate on the pairs (V_{d1},V_d) and (V_{d1},V_{d2}), to work with the first pair is found to be more convenient in order to interpret the plasma response. (In addition, since the third electrode can be placed at any axial location within the chamber, we will avoid the names ionization and acceleration voltages for V_{d1} and V_{d2}, respectively, used by some authors.)

(3) The currents exchanged at the intermediate electrode and at the external cathode, I_{d1} and I_{d2}, respectively, are obtained as a part of the plasma/thruster response. The cathode current I_{d2} is positive, but I_{d1} can either be positive or negative. The total discharge current through the anode is $I_d=I_{d1}+I_{d2}$.

(4) The voltages applied at each stage and the *r*-averaged values of the plasma potential at sections A,R, and P satisfying

$$\phi_A-\phi_R=V_{d1}-V_{\rm int}(I_{d1}),\quad \phi_A-\phi_P=V_d-V_{\rm cat}(I_{d2}). \tag{3}$$

Here, $V_{\rm int}$ and $V_{\rm cat}$ are the differences between the potentials of the respective electrodes and the *r*-averaged plasma potentials at sections R and P, respectively. The effective current–voltage curves of the electrodes, $V_{\rm cat}(I_{d2})$ and $V_{\rm int}(I_{d1})$, are supposed to be known. In general, the external cathode is of the hollow-cathode type and should work in the spot mode, characterized by emitting a high electron current with a relatively low potential voltage, $V_{\rm cat}\sim 15$–20 V. The other function, $V_{\rm int}(I_{d1})$, depends on the kind of electrode used. Only the ideal, zero-impedance cases (i.e., $V_{\rm cat},V_{\rm int}\ll V_d$) are treated in the present paper.

The rest of the hypotheses of the two-stage model are the same as the ones used in the single-stage model of Ref. 10. Unless otherwise stated, the nomenclature is the same too.

B. Equations

Except for a non-neutral sheath at the anode, the plasma is quasineutral and satisfies the set of equations

$$\frac{d\Gamma_{xi}}{dx}=-\frac{d\Gamma_{xn}}{dx}=S_i-S_w, \tag{4}$$

$$\frac{d\Gamma_{xe}}{dx}=S_i-S_w+S_{Pe}+S_{Re}, \tag{5}$$

$$\frac{d}{dx}(m_i v_{xi}\Gamma_{xi})=-en_eA\frac{d\phi}{dx}+m_i(v_{xn}S_i-v_{xi}S_w), \tag{6}$$

$$\frac{d}{dx}(m_i v_{xn}\Gamma_{xn})=m_i(v_{xnw}S_w-v_{xn}S_i), \tag{7}$$

$$0=-v_{xe}\omega_e-\nu_e v_{\theta e}, \tag{8}$$

$$0=-\frac{d}{dx}n_eT_e+en_e\frac{d\phi}{dx}+\omega_e m_e n_e v_{\theta e}, \tag{9}$$

$$\frac{d}{dx}\left(\frac{5}{2}T_e\Gamma_{xe}+q_{xe}A\right)=e\Gamma_{xe}\frac{d\phi}{dx}-\alpha_i E_i S_i-\beta_e T_e S_w+\frac{5}{2}T_P S_{Pe}+\frac{5}{2}T_R S_{Re}, \tag{10}$$

$$\frac{dT_e}{dx}=-\frac{2m_e\omega_e^2}{5n_eT_e\nu_e}q_{xe}. \tag{11}$$

Here, $m_\alpha,n_\alpha,T_\alpha$, and v_α, with $\alpha=i,e,n$, have the conventional meaning, q_{xe} is the axial heat conduction flux for the electrons, and $\Gamma_{x\alpha}=An_\alpha v_{x\alpha}$ are the particle axial flows. The four source terms for plasma production,

$$S_i=An_e\nu_i,\quad S_{Re}=\delta(x-x_R)I_{d1}/e,$$

$$S_w=An_e\nu_w,\quad S_{Pe}=\delta(x-x_P)I_{d2}/e, \tag{12}$$

represent the ionization, wall recombination, and electron emission at the electrode and the cathode, respectively; and $\delta(x)$ is the Dirac function. Notice that the 1D model treats similarly the volumetric term S_i and the other three terms, which model the contributions of the walls and electrodes. In Eq. (7), v_{xnw} is the average axial velocity of the neutrals generated by wall recombination. In Eq. (8),

$$\nu_e=\nu_{en}+\nu_{ei}+\beta_m\nu_w+\alpha_{ano}\omega_e \tag{13}$$

is the perpendicular collision frequency for electrons, which includes the effects of collisions with neutrals and ions,

secondary/primary electron exchanges at the lateral walls ("wall collisions"), and anomalous diffusion. In Eq. (10), T_R and T_P are the temperatures of the electrons exchanged at electrodes R and P, respectively; $\alpha_i E_i$ is the ionization energy cost (per ion); and $\beta_e T_e S_w$ represents the electron energy cost due to the interaction with the lateral walls. Expressions for $\nu_i, \nu_w, \nu_e, \alpha_i, \beta_m, \beta_e$, and υ_{xnw} can be obtained from Ref. 10.

From the continuity equations the axial flows satisfy

$$\Gamma_{xi}(x) + \Gamma_{xn}(x) = \dot{m}_A/m_i, \tag{14}$$

$$\Gamma_{xi}(x) - \Gamma_{xe}(x) = \begin{cases} I_d/e, & x < x_R, \\ I_{d2}/e, & x_R < x < x_P, \end{cases} \tag{15}$$

with $\dot{m}_A$ is the anode mass flow.

C. Jump conditions across the intermediate electrode

In the limit of a thin electrode expressed by condition (2), certain plasma magnitudes experiment a jump across the electrode location $x=x_R$. These jumps are determined from integrating the plasma equations from x_R^- to x_R^+. Notice that the first part of condition (2) implies that the discharge can afford the exchange of electric current at point R without creating a non-neutral double layer. Thus, any possible jump of the electric potential across point R must come out from the plasma quasineutral equations.

In the model we are considering, only the electron equations for the particle number and energy, Eqs. (5) and (10), are affected by the exchange of current at the intermediate electrode. Then, the integration of the equations across point R yields that υ_{xi}, n_e, T_e, and ϕ remain constant, whereas the jumps of the electron axial flows of particles and energy satisfy

$$\Gamma_{xeR}^+ - \Gamma_{xeR}^- = I_{d1}/e, \tag{16}$$

$$(q_{xeR}^+ - q_{xeR}^-)A_c = (T_R - T_{eR})5I_{d1}/2e, \tag{17}$$

with T_{eR} the electron temperature at point R and T_R the temperature of the electrons exchanged at the intermediate electrode. These equations express the conservation of the electron density and energy across the electrode location. Since $n_{eR}^+ = n_{eR}^-$, the jump of the electron current implies a jump of the electron axial velocity,

$$\upsilon_{xeR}^+ - \upsilon_{xeR}^- = I_{d1}/en_{eR}A_c \tag{18}$$

(notice that $\upsilon_{xe} < 0$).

D. Boundary conditions and structure of the discharge

The boundary conditions of the plasma equations for the two-stage case consist of those ones of the single-stage model plus the above jump conditions across point R. In the limit of zero intermediate current, $I_{d1}=0$, we pretend that the two-stage model recovers the *normal operation class* of solutions of Ref. 10. These present an axial structure consisting of the regions sketched in Fig. 1.

First, there is the negative anode sheath (region AB). The sheath potential, $\phi_{AB} \equiv \phi_B - \phi_A > 0$, is self-adjusted in order that the electron flow from the channel is the flow collected by the anode. The sheath/plasma transition (point B) is defined by a sonic Bohm condition on the ion reverse flow.

According to Ref. 10, the normal operation class of solutions exists only for the ion reverse current at the anode, $I_{iA} = e\Gamma_{xiA}$, satisfying

$$0.514 \times 10^{-2} < -I_{iA}/I_d < 11.4 \times 10^{-2}. \tag{19}$$

The lower limit of $|I_{iA}|$ corresponds to $\phi_{AB}=0$, that is, to the vanishing of the negative anode sheath. The upper limit corresponds to plasma flow conditions that seem not allowing a stationary presheath/sheath transition.[13] Therefore, the range defined by Eq. (19) is independent of any current exchange at an intermediate electrode and applies to two-stage operation too.

Points D and S in Fig. 1 correspond to zero and (forward) sonic ion velocities and are determined as part of the solution. Points E and P define the chamber exit surface and the beam neutralization surface. Region BD is the ion backstreaming region, which is characterized by a large pressure gradient, a near-zero electric field, and weak gas ionization. Region DS is the main ionization region and regions SE and EP are the internal and external acceleration regions, where most of the electric potential drop takes place. Ionization and wall-recombination frequencies tend to compensate each other in the acceleration regions;[10] therefore, ion and electron flows are almost constant there. Notice that magnetic effects are still significant in the external acceleration region EP.

Point S is determined as part of the solution and its location changes with the parameters controlling the thruster operation point. The model admits to place the third electrode (point R) anywhere inside the chamber, so that point S can be at any side of the electrode R. Nevertheless, we will deal mainly with parametric regions where point S is located inwards of point R since for an electron-emitting electrode, this assures that the intermediate current is used mainly to ionize the gas. Notice that Fruchtman *et al.*[9] claimed that the operation of the third electrode forces an abrupt sonic transition to occur exactly at the electrode location, and thus *imposed* the condition $x_R=x_S$ to all their two-stage solutions.

E. Input parameters for the integration

The geometrical, operational, and phenomenological parameters needed to integrate the two-stage model are the following:

(1) The chamber dimensions: radial width h_c, radial area A_c, and axial length L_c (we take $x_A=0$ and $x_E=L_c$).
(2) The distance between the chamber exit and the neutralization surface, $L_{EP} \equiv x_P - x_E$.
(3) The location of the intermediate electrode, $L_{AR} \equiv x_R$.
(4) The temperature T_1 of the primary electrons that produces a 100% SEE yield from the walls. The model yielding Eq. (A12) of Ref. 10 is used to compute the effective SEE yield.
(5) The anode mass flow rate $\dot{m}_A$ and the average axial velocity of the emitted gas, υ_{xnA}.
(6) The total and inner-stage voltages, V_d and V_{d1}.

(7) The temperature of the electrons emitted by the cathode, T_P. Since all electrons at point P come from the cathode, one has $T_{eP}=T_P$.
(8) The temperature of the intermediate electron current, T_R. We take $T_R=T_{eR}$ for an electron-collecting electrode and $T_R=T_P$ for an electron-emitting one.
(9) Three empirical parameters: the Bohm parameter measuring the level of turbulent diffusion [$\alpha_{\rm ano}$ in Eq. (A23) of Ref. 10]; the plasma-wall-recombination factor [$\tilde{\nu}_w$ in Eq. (A6) of Ref. 10]; and the accommodation factor for the axial velocity of the recombined ions [a_w in Eq. (13) of Ref. 10].
(10) The axial profile of the radial magnetic field, $B_r(x)=B_{\max}b_r(x)$. The shape of this profile, $b_r(x)$, is kept fixed, whereas the maximum magnetic-field strength, B_{max}, is adjusted in order that condition (19) is satisfied (i.e., the solution presents a negative anode sheath). For the rest of the parameters given, this restricts the range of values of the maximum magnetic-field strength B_{max} to a thin variation band (of around a 10%, according to Fig. 6 of Ref. 13).

III. ANALYTICAL RELATIONS OF INTEREST

A. Energy balance

The external electrical power spent in a two-stage discharge is

$$P_d = I_d V_{d1} + I_{d2} V_{d2} = I_d V_d - I_{d1} V_{d2}. \tag{20}$$

Defining

$$P_\alpha(x) = \Gamma_{x\alpha}\left(\frac{1}{2}m_i v_{x\alpha}^2 + \frac{5}{2}T_\alpha\right) + q_{x\alpha}A \tag{21}$$

as the axial energy flow carried by species α, the useful power extracted from the thruster is

$$P_{\rm use} = P_{iP} + P_{nP} \simeq \sum_{\alpha=i,n} \frac{1}{2}\dot{m}_{\alpha P} v_{x\alpha P}^2. \tag{22}$$

(Since our model is not reliable at the far plume, we do not integrate beyond point P and thrust and useful power will be computed from the plasma values at point P.) The r-averaged energy balance of the whole plasma allows us to evaluate the different contributions to the energy losses, $P_{\rm loss}=P_d-P_{\rm use}$. Equation (10) yields the axial variation of the energy flow of the electron population. From the equations of ions and neutrals the total energy flow of ions and neutrals satisfies

$$\frac{d}{dx}(P_i+P_n) = -e\Gamma_{xi}\frac{d\phi}{dx} - S_w\left[\frac{5}{2}T_i + \frac{1}{2}m_i(v_{xi}^2 - v_{xnw}^2)\right] \tag{23}$$

(the ion temperature T_i, neglected in Eq. (6), is included here for a consistent balance of the total energy of the heavy species). Adding Eqs. (10) and (23) and integrating for each stage of the discharge, one has

$$I_d\phi_{RA} = (P_i+P_n+P_e)\big|_A^{R^+} + \int_A^R (Q_{\rm wall}+Q_{\rm ion})dx + \frac{5T_R}{2e}I_{d1}, \tag{24}$$

$$I_{d2}\phi_{PR} = (P_i+P_n+P_e)\big|_{R^+}^{P} + \int_R^P (Q_{\rm wall}+Q_{\rm ion})dx + \frac{5T_P}{2e}I_{d2}, \tag{25}$$

with

$$Q_{\rm ion} = \alpha_i E_i S_i, \quad Q_{\rm wall} = \left[\frac{1}{2}m_i(v_{xi}^2 - v_{xnw}^2) + \frac{5}{2}T_i + \beta_e T_e\right]S_w, \tag{26}$$

the local losses (per unit of axial length) due to ionization and plasma interaction with the lateral walls, respectively. The dimensionless parameter β_e, measuring the radial losses to the walls, increases dramatically in zones where the SEE yield approaches 100% (i.e., $T_e \simeq T_1$) and the lateral sheaths become space-charge saturated.[12]

Adding Eqs. (3), (24), and (25), the energy losses can be written as

$$P_{\rm loss} = P_{\rm ion} + P_{\rm wall} + P_{\rm ano} + P_{\rm int} + P_{\rm plu}, \tag{27}$$

where

$$P_{\rm ion} = \int_A^P Q_{\rm ion}dx, \quad P_{\rm wall} = \int_A^P Q_{\rm wall}dx, \tag{28}$$

$$P_{\rm ano} = -(P_i+P_n+P_e)|_A, \quad P_{\rm int} = I_{d1}\left(V_{\rm int} - \frac{5}{2}\frac{T_R}{e}\right),$$

$$P_{\rm plu} = I_{d2}\left(V_{\rm cat} - \frac{5}{2}\frac{T_P}{e}\right) + P_{eP},$$

represent the ionization, heat deposited at the lateral walls, heat deposition at the anode, losses due to the current exchanged at the intermediate electrode, and losses in the near plume, respectively.

B. Partial efficiencies

The thrust satisfies

$$F = \sum_{\alpha=i,n} \dot{m}_{\alpha P} v_{x\alpha P}. \tag{29}$$

Partial efficiencies of interest are defined in Ref. 14:

$$\eta = F^2/2\dot{m}_A P_d, \quad \eta_{\rm prop} = P_{\rm use}/P_d, \quad \eta_u = \dot{m}_{iP}/\dot{m}_A, \tag{30}$$

$$\eta_{\rm vol} = m_i v_{xiP}^2/2eV_d, \quad \eta_{\rm cur} = I_{iP}V_d/P_d,$$

mean thrust and propulsive efficiencies, propellant, voltage, and current utilizations, respectively. The difference between the thrust and propulsive efficiencies comes from the incomplete ionization, which means that the ejected plasma beam

includes two heavy species with different velocities. One has[14]

$$\eta \simeq \eta_u \eta_{\text{prop}}, \quad \eta_{\text{prop}} \simeq \eta_{\text{vol}} \eta_{\text{cur}}, \quad \eta_{\text{cur}} \simeq \eta_u I_m V_d / P_d, \tag{31}$$

with $I_m = e\dot{m}_A/m_i$ and $I_m V_d$ the ideal maxima of the ion current and useful power, respectively (for given values of the two main operation parameters, $\dot{m}_A$ and V_d). The analysis of single-stage discharges shows that $\dot{m}_A$ and V_d affect mildly both η_{vol} and η_u (within the operation regime of interest to us).[14] Therefore, the most promising way of enhancing η is to increase η_{cur} by reducing the energy losses and thus P_d. Since P_{ano} and P_{plu} are small and there is a little margin to decrease the ionization losses, a two-stage design must focus on reducing P_{wall}. This can be accomplished by limiting the plasma temperature in the acceleration regions in order to avoid the presence of regions with charge-saturated sheaths, which lead to large energy depositions at the walls.

C. Scaling laws for the magnetic field

Once an axial shape of the magnetic field is selected, the value of the magnetic-field strength $B_{\max}$ is adjusted in order to provide the correct diffusion of the axial electron flow across the chamber [and a reverse flow of ions within the range of Eq. (19)]. Approximate solutions of the plasma equations, discussed in Ref. 14 give the scaling law for the parametric dependence of $B_{\max}$ on V_d for a single-stage operation. Using the same approximations, scaling laws for the first and second acceleration regions (regions *SR* and *RP* in Fig. 1) are

$$\sqrt{\frac{2eV_d}{m_i}} - \sqrt{\frac{2eV_{d1}}{m_i}} \simeq \frac{I_{d2} - I_{iP}}{I_{iP}} \{\bar{\nu}_d\}_{RP} L_{RP}, \tag{32}$$

$$\sqrt{\frac{2eV_{d1}}{m_i}} - \sqrt{\frac{2e\phi_{SA}}{m_i}} \simeq \frac{I_d - I_{iP}}{I_{iP}} \{\bar{\nu}_d\}_{SR} L_{SR}, \tag{33}$$

where {} means the average value over the respective region;

$$\bar{\nu}_d = \frac{m_e}{m_i} \frac{\omega_e^2}{\nu_e} \tag{34}$$

is a normalized perpendicular collision frequency of electrons (with $\bar{\nu}_d \propto B_{\max}/\alpha_{\text{ano}}$ if turbulent diffusion dominates); $L_{RP} \equiv x_P - x_R$ is known; and $L_{SR} = x_R - x_S$ changes with the operation point. To complete these two scaling laws we need a third one for the length of the ionization and backstreaming regions, $L_{AS} = L_{AR} - L_{SR}$. There is no simple, correct expression for the scaling of that length but

$$L_{AS} \propto \{\bar{\nu}_d \nu_i\}_{AS}^{-1/2} \tag{35}$$

can be accepted as a rough estimate.[14,15] These three scaling laws will be used later to interpret the plasma response and the dependence of $B_{\max}$ on V_{d1} and x_R.

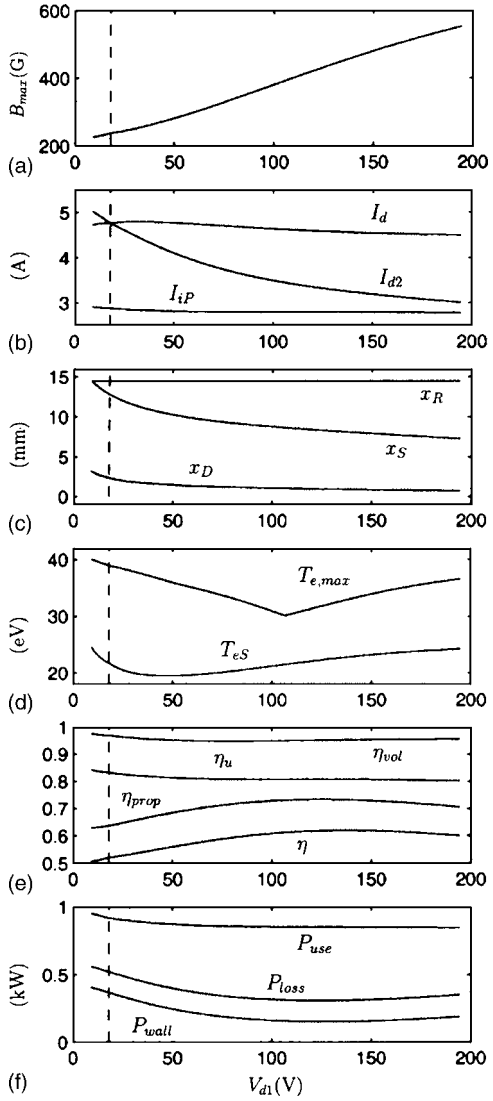

FIG. 2. Evolution of thruster parameters with the inner-stage voltage when the intermediate electrode is placed at $x_R = 14.5$ mm. Other input parameters are $L_c = 25$ mm, $L_{EP} = 8.5$ mm, $A_c = 40$ cm^2, $V_d = 296$ V, $\dot{m} = 4.78$ mg/s, $T_{eP} = 4.4$ eV, $\alpha_{\text{ano}} \simeq 0.0124$, $T_1 \simeq 39.93$ eV, and $\tilde{\nu}_w \simeq 0.191$. The function $B_{\max}(V_{d1})$, in plot (a), is an input too. The dashed vertical line corresponds to single-stage operation (or floating-case of the intermediate electrode).

IV. PARAMETRIC INVESTIGATION OF THE TWO-STAGE OPERATION

A. Evolution with the intermediate voltage

Numerical results are presented for the same thruster considered in Refs. 10 and 14, which simulates a SPT 100. Figures 2(a)–2(f) analyze the influence of the first-stage voltage V_{d1} on the performances for a fixed position of the intermediate electrode. The total discharge voltage and the mass flow are kept constant so that the variation on the discharge power is related directly to the exchange of current at the electrode. Main input parameters of the thruster are listed in the caption of Fig. 2; the chamber length is $L_c = 25$ mm and the electrode is placed at 14.5 mm from the anode. The axial shape of the magnetic field $b_r(x)$ is the same as the one plotted in Fig. 2 of Ref. 10. For each operation point, the magnetic-field strength, Fig. 2(a), has been adjusted in order that $-I_{iA}/I_d$ lie in the interval 0.012–0.025.

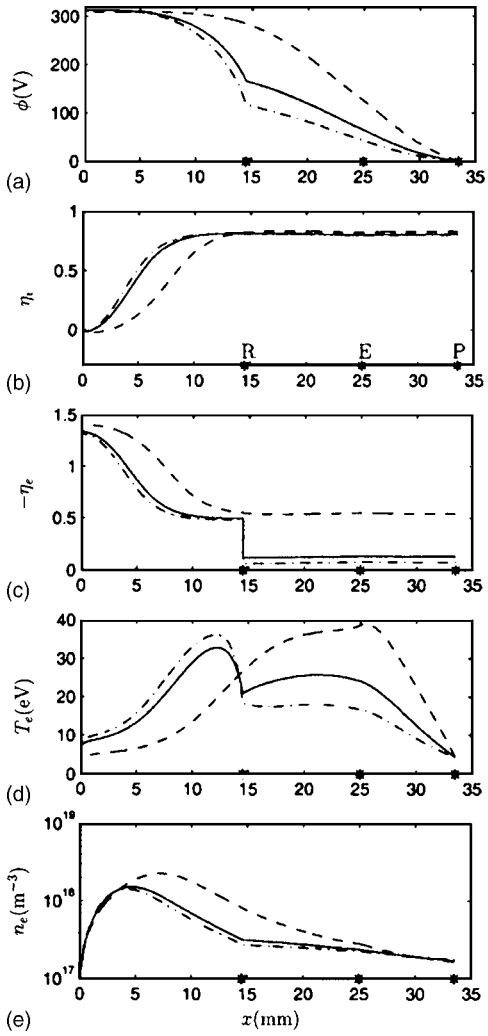

FIG. 3. Axial response for three particular points of Fig. 2; $V_{d1}=18$ V (dashed lines), 137 V (solid lines), and 196 V (dash-and-dot lines). The intermediate current are $I_{d1}=0$, 1.3, and 1.5 A, respectively. The asterisks represent points R,E, and P. Plots (b) and (c) show dimensionless particle flows of ions and electrons, $\eta_\alpha(x)=m_i\Gamma_{x\alpha}(x)/\dot{m}_A, \alpha=i,e$.

Figures 3(a)–3(e) depict the axial profiles of the plasma response for three particular points of Fig. 2. One-stage operation ($I_{d1}=0$ and dashed-line curves of Fig. 3) is achieved for $V_{d1}=18$ V and yields a thrust efficiency of 52%. As V_{d1} is increased from that floating value, electron current is emitted into the discharge at point R. The solid-line curves of Fig. 3 depict the discharge response for $V_{d1}=137$ V (i.e., $V_{d1}/V_d \simeq 46\%$), when the intermediate current is $I_{d1}\simeq 1.3$ A and the thrust efficiency is maximum and is equal to 62%. The dash-and-dot curves of Fig. 3 plot the response for $V_{d1}=196$ V when $I_{d1}\simeq 1.5$ A and $\eta\simeq 60\%$.

The evolution of $I_{d1}(V_{d1})=I_d-I_{d2}$ can be seen in Fig. 2(b). As both the total discharge current and the ion final current, I_d and I_{iP}, are found to change weakly with V_{d1}, it turns out that the increments of I_{d1} are followed by decrements of the same magnitude of both the electron current emitted by the cathode, I_{d2}, and the outer-stage reverse current of electrons, $I_{d2}-I_{iP}$. For the cases plotted in Fig. 3 and for V_{d1} increasing, this reverse electron current decreases from 1.88 to 0.46 A and 0.25 A. Since a certain reverse electron current is needed to sustain the quasineutral discharge in the outer stage, the low value of $I_{d2}-I_{iP}$ for $V_{d1}=196$ V could explain partially the numerical difficulties we have found to obtain solutions for larger values of V_{d1}. (To this respect, we do not see any theoretical obstacle in the model preventing the existence of solutions for higher values of V_{d1}. Indeed, the model would allow V_{d1} to approach V_d and the intermediate electrode to become the effective cathode.)

At the floating-potential (or single-stage) case, the ionization region ends at $x_S=12.9$ mm, near the location of the intermediate electrode. The potential drop in the backstreaming and ionization regions is practically independent of the intermediate electrode operation; one has $\phi_{SA}\equiv\phi_A-\phi_S \sim T_{eS}/2e$ or more specifically, $\phi_{SA}=7.4$ and 6.9 V for $V_{d1}=18$ and 137 V, respectively. Since ϕ_{SA} is small, the potential drop in the inner acceleration region, $\phi_{RS}\equiv\phi_S-\phi_R$, tends to be proportional to V_{d1}. Then, as V_{d1} becomes larger and in order to accommodate the larger potential difference ϕ_{RS}, point S moves away from point R [Fig. 2(c)]. At the maximum efficiency case ($V_{d1}=137$ V) point S is placed at $x_S=8.1$ mm, almost at mid-distance from the anode and the intermediate electrode.

Figure 2(e) shows that the propellant utilization is affected weakly by the intermediate electrode operation (in agreement with the conclusions of Ref. 10). The small variation of $\eta_u(V_{d1})$ seems to be due to the variation of the maximum electron density in the ionization region [Fig. 3(e)]. Then, $\eta\simeq\eta_u\eta_{\text{prop}}$ presents the same evolution with V_{d1} than η_{prop} [Fig. 2(e)]. The useful power and the power losses, which determine the propulsive efficiency, are shown in Fig. 2(f). We observe that P_{wall} is the dominant contribution to P_{loss} and P_{use} varies weakly with the intermediate electrode operation. As a result, the maxima of $\eta_{\text{prop}}(V_{d1})$ and $\eta(V_{d1})$ correspond to the minimum of $P_{\text{wall}}(V_{d1})$ approximately.

As commented in Sec. III, P_{wall} is strongly affected by the temperature profile. Since the increase of V_{d1} means a reduction of both V_{d2} and I_{d2}, the plasma heating, the electron temperature, and the wall energy losses will be lower in the outer stage (region RP). But, simultaneously, the increase of V_{d1} means a larger plasma heating in the inner acceleration region SR. As a consequence, for large enough values of V_{d1}, the charge saturation of the lateral sheaths tends to disappear from region RP and to appear in region SR. This is well illustrated by the three temperature profiles plotted in Fig. 3(d) and the behavior of the maximum electron temperature $T_{e,\max}(V_{d1})$, in Fig. 2(d). The change of the tendency of $T_{e,\max}(V_{d1})$ at $V_{d1}\sim 105$ V is due to the change on the location of the maximum temperature, from region RP to region SR. The fact that wall energy losses increase largely when there is a large axial zone with sheath saturation, explains that the minima of $T_{e,\max}(V_{d1})$ and $P_{\text{wall}}(V_{d1})$ [Figs. 2(d) and 2(f)], are close to each other. The main conclusion is that maximum efficiency is obtained when the two-stage operation generates a rather flat temperature profile, with few zones with charge-saturated sheaths.

The small variation of the total discharge current with V_{d1}, Fig. 2(b), is due to the following: In the one-stage operation (and for $\dot{m}_A$ given), I_d is determined mainly by the

amount of power losses through the expression $I_d \simeq \eta_u \eta_{\rm vol}(e\dot{m}_A/m_i)+P_{\rm loss}/V_d$. In two-stage operation, this expression becomes

$$I_d \simeq \eta_u \eta_{\rm vol}\frac{e\dot{m}_A}{m_i}+\frac{P_{\rm loss}+I_{d1}V_{d2}}{V_d}. \tag{36}$$

Thus, from Eqs. (20) and (36), $I_d \approx$ constant means that the gain in the discharge power is $I_{d1}V_{d2}$ and this comes almost entirely from reducing $P_{\rm wall}$. Since $I_{d1}V_{d2}$ is of the order of the reduction of Joule heating in the outer stage, it turns out that $I_d \approx$ constant is mainly the result of the balance between Joule heating and wall energy losses in the outer stage.

Figure 2(a) shows that a significant increase of $B_{\max}$ with V_{d1} is needed to keep the two-stage discharge within the normal operation class (i.e., with a negative anode sheath and an ion backstreaming region); $B_{\max}$ doubles from a single-stage to an efficient two-stage operation. Equation (33) provides the basic relationship to understand the behavior of $B_{\max}(V_{d1})$: The increase of V_{d1} requires to increase $(L_{AR}-L_{AS})B_{\max}$ and this is accomplished by a larger $B_{\max}$ [which according to Eq. (35) yields a shorter L_{AS} too]. The plasma equations leading to Eq. (33) [see Eq. (9) of Ref. 14] provide the physical explanation in terms of plasma magnitudes. A larger potential jump between R and S means a larger increment of v_{xi} and, because of plasma quasineutrality, of v_{xe} too. The increment of v_{xe} satisfies

$$\Delta v_{xe} \sim -\int_S^R dx\,\bar{\nu}_d \Gamma_{xe}^2/\Gamma_{xi}^2 \tag{37}$$

and thus is almost proportional to $\bar{\nu}_d$.

The variation of the magnetic-field strength affects the electron flow in the following way. In the outer stage, the balance between a larger $B_{\max}$ and lower electron current and electric field is given by Eq. (32), which basically states that

$$B_{\max} \propto \frac{V_d^{1/2}-V_{d1}^{1/2}}{I_{d2}-I_{iP}}. \tag{38}$$

In the ion backstreaming region, Eqs. (8) and (9) together with $I_d \approx$ constant indicate that the electron pressure increases nearly proportional to the magnetic field,

$$\{n_e T_e\}_{BD} \propto \{|\mathbf{B}|\}_{BD} \propto B_{\max}; \tag{39}$$

Fig. 3 shows that this pressure increment comes from the temperature increase in the near-anode region.

There are no experimental data that could guide us on the variation of the anomalous diffusion parameter $\alpha_{\rm ano}$ with the operation conditions of a two-stage thruster. Thus, we used the same value, $\alpha_{\rm ano} \simeq 1.24\%$, for all cases computed in the paper. (This value was adjusted in Ref. 10 by fitting single-stage solutions to the experimental results of the SPT-100 thruster.) However, results are valid for other values of $\alpha_{\rm ano}$ because $B_r(x)$ and $\alpha_{\rm ano}$ appear in the equations only in one parameter, the perpendicular collision frequency $\bar{\nu}_d$ defined in Eq. (34). Thus, any solution of the discharge computed here is valid for pairs $[B_r(x), \alpha_{\rm ano}]$ that keep $\bar{\nu}_d(x)$ invariant. When turbulent diffusion dominates over the rest of the collisional effects, that condition reduces to keeping $B_r(x)\alpha_{\rm ano}^{-1}$ invariant. Then, where $\alpha_{\rm ano}$ vary with the operation point, Fig. 2(a) would represent the way the ratio $B_{\max}\alpha_{\rm ano}^{-1}$ (instead of $B_{\max}$) needs to be adjusted; the same is true with Eqs. (38) and (39). Therefore, the turbulent diffusion level affects the magnetic-field strength that must be applied, but not the maximum efficiency gain that can be achieved.

B. The electron-collecting mode

Figure 2 also includes results for the intermediate electrode operating as an electron collector. When V_{d1} decreases from the floating value of 17.9 V, the current at the intermediate electrode I_{d1} starts to be negative. Our results show that this operation regime is clearly disadvantageous; part of the reverse electron current emitted by the external cathode is heated at the outer stage and collected back at point R without performing any useful task (i.e., ionization). Figure 2(d)–2(f) illustrate the extra heating of the plasma with a negative impact on energy losses and efficiency. At the same time, a lower potential drop in region AR does not produce any relevant enhancement of the propellant utilization.

With respect to the position of the ionization region, Fig. 2(c) shows that, as V_{d1} decreases, point S approaches the intermediate electrode and eventually crosses it; one has $V_{d1}=9.1$ V and $I_{d1}=-0.3$ A when $x_S=x_R=14.5$ mm. Computations with point S outwards of point R were not performed since new and interesting results were not foreseen. When the intermediate electrode is placed upstream of the ionization region (i.e., $x_D>x_R$), this electrode is expected to act as the main anode; this could be the situation in some experiments with the P5-2.[7]

Fruchtman *et al.*[9] found that the thruster efficiency can be improved significantly by using an electron-collecting electrode. The discrepancy with our conclusions is explained by the differences in both the model and the cases presented. First they consider single-stage cases where ionization covers the whole channel and the values of $\eta_{\rm vol}$ and η_u are relatively low (whereas we depart from single-stage cases with $\eta_u>80\%$ and $\eta_{\rm vol}>90\%$). For such cases the main role of the intermediate electrode seems to modify the electric potential profile in order to force the ionization region to occupy only one part of the channel, thus enhancing the propellant and voltage utilizations. Second, although recognizing the importance of the temperature evolution along the chamber, they take, for simplicity, $T_e(x)$ (and the ionization rate) to be constant and the *same* for single-stage and two-stage operations. Thus, by avoiding to solve the energy equation, it is not realized that the energy losses tend to increase in the electron-collecting mode, penalizing the current utilization and thrust efficiency.

C. Influence of the location of the intermediate electrode

Figures 4(a)–4(f) present the results of a biparametric study on the influence of the position and the bias voltage of the intermediate electrode, x_R and V_{d1}, on the thruster performance (for fixed values of V_d and $\dot{m}_A$). The investigation covers a wide range of variation (over 50%) of both V_{d1}/V_d and x_R/L_c. The solid thick lines represent the single-stage operation or floating-potential case for the intermediate elec-

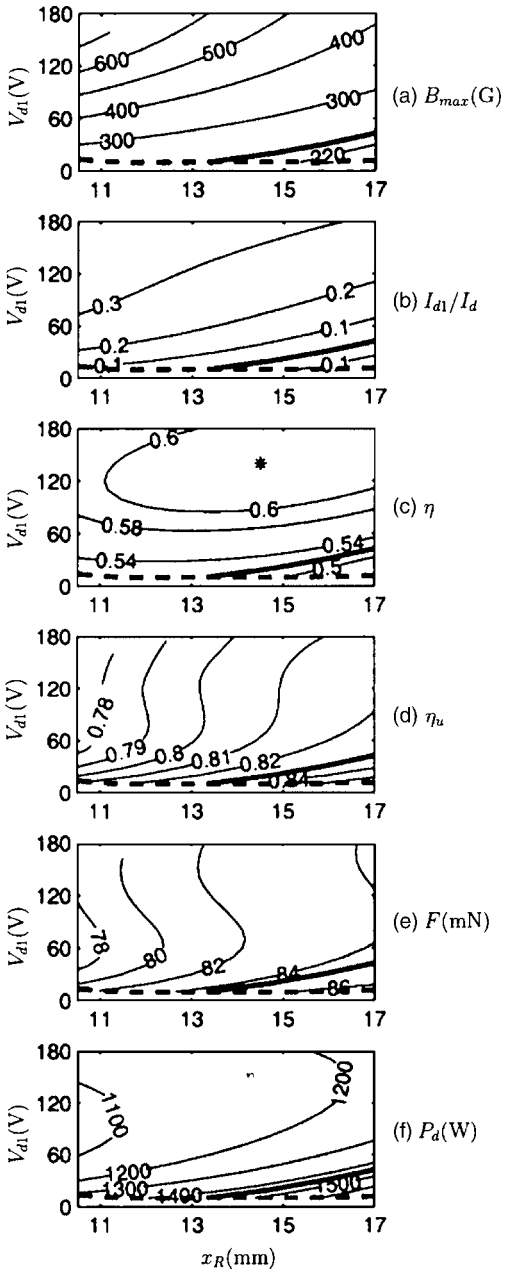

FIG. 4. Level lines of main parameters characterizing the thruster response as functions of the third-electrode position and inner-stage voltage, x_R and V_{d1}, respectively. The rest of thruster parameters are as in Fig. 2, in particular, V_d=296 V, $\dot{m}_A$=4.78 mg/s, and $\alpha_{\text{ano}} \simeq 0.0124$. Thick solid lines represent single-stage operation or the floating case of the third electrode. Thick dashed lines correspond to $x_R = x_S$.

trode. The dashed thick lines correspond to $x_R = x_S$, when the ion sonic point lies exactly at the intermediate electrode position. The change on the magnitude of the magnetic-field profile in Fig. 4(a) reflects the adjustment required by $B_{\max}(x_R, V_{d1})$ for the plasma discharge to lie within the normal operation regime.

Figure 4(b) plots the fraction of the electron current exchanged at the intermediate electrode, I_{d1}/I_d, which reaches up to a 30%. Figure 4(c) plots the evolution of the efficiency $\eta(x_R, V_{d1})$. The asterisk represents the point of maximum efficiency, about 62%, which is reached for x_R=14.5 mm and V_{d1}=137 V (the solid-line case of Fig. 3). Therefore, for this thruster and $V_d \sim 300$ V, the ideal two-stage discharge model yields 19% of efficiency improvement with respect to single-stage operation. As important as this result is the fact that $\eta(x_R, V_{d1})$ remains close to that maximum for a wide interval of voltages and positions of the electrode. For instance, one has $\eta > 0.60$ for V_{d1}=125 V and x_R in the interval 11–18 mm, or for x_R=14.5 mm and V_{d1} in the range 100–200 V.

We saw in Sec. IV A that η_u is practically independent of V_{d1} (in the region of interest, $V_{d1} \sim 100$–150 V). Figure 4(d) shows that η_u depends weakly on x_R. Then, the behavior of $\eta_{\text{prop}}(x_R, V_{d1}) \simeq \eta/\eta_u$ is similar to that of $\eta(x_R, V_{d1})$. Since the voltage utilization is always high, the behavior of the thrust function $F(x_R, V_{d1})$, Fig. 4(e), is similar to that of η_u. More outward electrode positions yield larger values of F, but larger values of P_d too, Fig. 4(f). To maximize the thrust and minimize the discharge power, the inner-stage voltage must be in the interval $V_{d1} \sim 120$–150 V.

The common two-stage design, which places the intermediate electrode between the ionization and acceleration regions and applies a low inner-stage voltage,[1] would correspond here to $V_{d1} \sim 20$–40 V and $x_R \sim x_S$. Figure 5(a)–5(e) shows the two-stage performance for V_{d1}=30 V when the location of the third electrode varies from x_R=10 to 17 mm. As the electrode is placed inwards, the relative emission current increases up to 20%. This leads to about 10% increment of the propulsive efficiency, but also to a reduction of both η_u and η_{vol}. As a result of these opposite trends the gain in thrust efficiency is rather modest (from 52% to 54%). Again for this case, the electrode operation as an electron collector (for $x_R > 16$ mm) leads to a decrease of the performances; η_u and η_{vol} increase, in agreement with Ref. 9, but, because of energy losses, η_{prop} decreases in a larger proportion.

Fruchtman and Fisch[8] used a simple 1D model of the acceleration region to determine the optimal location and voltage of an intermediate electrode. They found that the maximum efficiency gain of a *generic* two-stage thruster is about 6% for low η, and reduces to about 3% for η=52%. We try to explain next the discrepancy between this universal value and the 19% of gain for the particular thruster treated in Fig. 4. First, their model ignores completely the ionization and backstreaming regions; with our notation, it can be said that they assume $L_{AS}=0$, $\phi_{AS}=0$, and $\eta \propto \eta_{\text{cur}}$. Second, in order to determine the optimal third-electrode conditions they *assume* that I_{iP} and $\bar{\nu}_d$ are independent of V_{d1} and x_R, whereas the discharge current I_d is a free parameter. With these simplifications and constraints, the optimal third-electrode parameters are

$$\frac{V_{d1}}{V_d} \sim 2\,\%\,, \quad \frac{\{\bar{\nu}_d\}_{SR} L_{SR}}{\{\bar{\nu}_d\}_{SP} L_{SP}} \sim 4.5\,\%\,,$$

values that differ strongly with ours in addition, the reverse electron current at the inner stage, $I_d - I_{iP}$, changes by more than a 300% from the single-stage case to their optimal two-stage case. Our model shows that the changes on the upstream regions and its coupling with the acceleration region cannot be neglected; for instance, the length L_{AS} is neither negligible nor constant. But the principal point explaining the large discrepancy with Fruchtman-Fisch lies in the assumptions made on I_d and $\bar{\nu}_d$. Our solutions for the whole

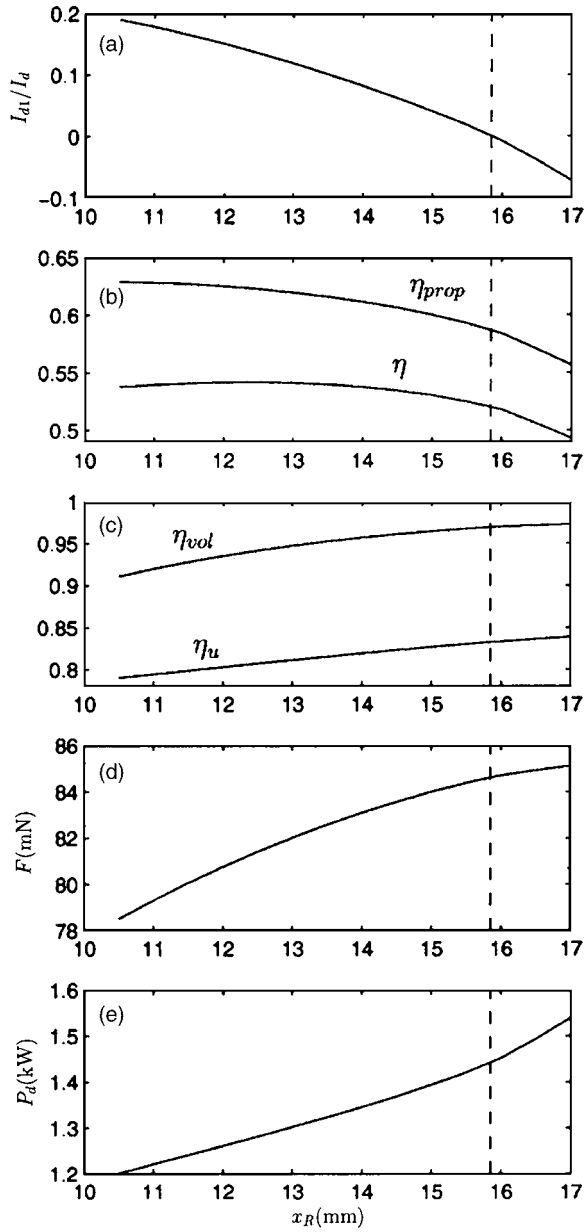

FIG. 5. Evolution of thruster parameters with the location of the third electrode for $V_{d1}=30$ V. The rest of thruster parameters are as in Fig. 2. The vertical, dashed line corresponds to the single-stage operation, $I_{d1}=0$.

channel *do show* that I_{iP} and I_d remain near constant for most third-electrode conditions, whereas $\bar{\nu}_d$ (i.e., $B_{\max}$) must be adjusted for each case. As commented before, the fact that I_d remains almost invariant is a consequence of the electron energy balance. Therefore, although the electron temperature is absent from the definition of $\eta_{\rm cur}$ and from Eqs. (32) and (33), the energy balance is essential in order to solve correctly the problem.

V. CONCLUSIONS

The present model of a two-stage discharge shows that a good electron-emitting electrode inserted in the acceleration region of the chamber enhances the thruster efficiency. The improvement is significant for thrusters where energy losses are dominated by the interaction with the lateral walls, like thrusters with long ceramic chambers (i.e., SPT-type) and operating at mid- and high-discharge voltages.

For the midpower, midvoltage thruster studied in this paper, the efficiency increases from 52% for single-stage operation to 62% for the best two-stage operation. As important as this increase is that the efficiency can be kept close to its maximum two-stage value for a relatively wide range of positions and voltages of the intermediate electrode. A two-parameter investigation on the influence of the electrode position and voltage on the performance of that specific thruster concludes that (i) the best location is at an intermediate point within the internal acceleration region and (ii) the optimum first-stage voltage is about 40%–50% of the total discharge voltage.

Two-stage designs and models have generally put the emphasis on improving the efficiency of the ion beam, which basically means to improve the propellant and voltage utilizations. On the contrary, our idea has been to depart from a single-stage design with high values of these ionization-related efficiencies and to focus on reducing the electron energy losses to the walls in the acceleration region. It turns out that the insertion of part of the electron reverse current near the ionization region reduces the temperature in the acceleration region without affecting practically the propellant and voltage utilizations. Maximum efficiency is obtained for a two-stage operation point where the profile of the electron temperature is rather flat and the temperature peak is near its minimum value, thus minimizing the zones with charge-saturated sheaths.

Other conclusions of the present study are the following: First, to solve the electron energy equation is essential to determine the thruster performances and thus constitutes a major advance over previous models. Second, the operation at different inner-stage voltages requires to adjust the strength of the magnetic field; to zeroth order, the magnetic strength increases inversely proportional to the electron reverse current in the outer stage. Third, two-stage discharges with low inner-stage voltages do not lead to relevant efficiency increments. And fourth, an electron-collecting electrode deteriorates the thruster efficiency, at least when the ionization process is already efficient in single-stage operation.

The present paper was aimed to understand the main physical aspects of two-stage discharges and to evaluate the improvements of efficiency. Certainly, several relevant aspects and modeling issues require further studies. First, there is the optimization of the thruster design, beyond determining the optimal position and voltage of the third electrode. In particular, the optimum axial shape of the magnetic field for two-stage operation should be investigated. This could differ from the single-stage one with its pronounced peak near the exit of the chamber and the peak of the electric field.

Second, a performance study for the operational range of the discharge voltages and mass flows is essential for two-stage thrusters envisaged for variable thrust operation. Two-stage operation is specifically proposed for the high specific impulse mode, when (if power is constant) the mass flow is lowest and the ionization process can become inefficient. For this case, two-stage operation could help to increase η_u too.

Third, there are limitations inherent to the 1D model that must be evaluated. In particular, 2D effects related to (i) the inner or outer location of the electrode and (ii) the topography of the magnetic-field lines could have a significant impact on the plasma response.

Fourth, the two-stage model must be extended to intermediate electrodes with nonzero impedance. The extension is simple for the case of low impedance if the current–voltage characteristic of the electrode is known. But the present model is not directly applicable to low emission and passive electrodes. In this last case, the electron-emission mode is in fact an ion-collection mode and requires to modify the ion conservation equation. The benefits of SPT-type thrusters with a intermediate passive electrode are dubious since the ion-collection regime seems to imply a reduction of the final ion-beam flow.

Fifth, for the two-stage thrusters discussed here, the efficiency gain is based mainly on the reduction of the wall energy losses. These are very sensitive to the plasma-wall interaction model and the uncertainties of this model are transferred directly to our results. Although the radial model of Ref. 12 provides a plausible and self-consistent physical view of that interaction, it is also known that it tends to overestimate the particle and energy losses.[10] One part of this seems to be due to the 2D ion dynamics but the main part is likely due to the assumption of a quasi-Maxwellian distribution function of primary electrons near the walls. Recent works[16,17] have suggested a strong distortion of the tail of the electron distribution caused by both magnetic mirroring and incomplete replenishment of the collected electrons. The recollection by the walls of part of the SEE can modify the energy losses too.[18] At present, the consequences of these phenomena on the different terms modeling the wall losses have been quantified only partially. The main issue is that a reduction of the relative weight of wall energy losses will possibly imply a reduction of the maximum efficiency gain obtained from two-stage thrusters.

Finally, attention must be paid to the technical aspects that can reduce and even cancel the benefits obtained from the improvement of the plasma performances. These technical issues would include, at least, (i) the power spent to heat the third electrode, (ii) the possible contamination of the chamber walls generated by electrode-eroded material,[19] (iii) the reduction of lifetime and reliability due to the more complex design and fabrication of the chamber, and (iv) the larger mass of the whole thruster.

ACKNOWLEDGMENTS

This research was sponsored by the Air Force Office of Scientific Research, Air Force Material Command, USAF under Grant No. FA8655-04-1-3003, and by the Ministerio de Educación y Ciencia of Spain (Project No. ESP2004-03093).

[1] H. Kaufman, AIAA J. **23**, 78 (1985).
[2] D. Jacobson, R. Jankovsky, V. Rawlin, and D. Manzella, *Proceedings of the 37th Joint Propulsion Conference*, Salt Lake City, UT, July 8–11, 2001 (American Institute of Aeronautics and Astronautics, Washington, DC, 2001), AIAA-2001-3777.
[3] A. Solodukhin, A. Semenkin, S. Tverdokhlebov, and A. Kochergin, *Proceedings of the 27th International Electric Propulsion Conference*, Pasadena, CA, Oct. 14–19, 2001 (Electric Rocket Propulsion Society, Cleveland, OH, 2001), IEPC-01-032.
[4] Y. Yamagiwa and K. Kuriki, J. Propul. Power **7**, 65 (1991).
[5] N. Fisch, Y. Raitses, L. Dorf, and A. Litvak, J. Appl. Phys. **89**, 2040 (2001).
[6] B. Pote and R. Tedrake, *Proceedings of the 27th International Electric Propulsion Conference*, Pasadena, CA, Oct. 14–19, 2001 (Electric Rocket Propulsion Society, Cleveland, OH, 2001), IEPC-01-035.
[7] R. Hofer, P. Peterson, A. Gallimore, and R. Jankovsky, *Proceedings of the 27th International Electric Propulsion Conference*, Pasadena, CA, Oct. 14–19, 2001 (Electric Rocket Propulsion Society, Cleveland, OH, 2001), IEPC-01-036.
[8] A. Fruchtman and N. Fisch, Phys. Plasmas **8**, 56 (2001).
[9] A. Fruchtman, N. Fisch, and Y. Raitses, Phys. Plasmas **8**, 1048 (2001).
[10] E. Ahedo, J. Gallardo, and M. Martínez-Sánchez, Phys. Plasmas **10**, 3397 (2003).
[11] G. Janes and R. Lowder, Phys. Fluids **9**, 1115 (1966).
[12] E. Ahedo, Phys. Plasmas **9**, 4340 (2002).
[13] E. Ahedo, J. Gallardo, and M. Martínez-Sánchez, Phys. Plasmas **9**, 4061 (2002).
[14] E. Ahedo and D. Escobar, J. Appl. Phys. **96**, 983 (2004).
[15] E. Ahedo, P. Martínez-Cerezo, and M. Martínez-Sánchez, Phys. Plasmas **8**, 3058 (2001).
[16] N. Meezan and M. Capelli, Phys. Rev. E **66**, 036401 (2002).
[17] K. Sullivan, J. Fox, O. Batischev, and M. Martínez-Sánchez, *Proceedings of the 40th Joint Propulsion Conference*, Fort Lauderdale, FL, July 11–14, 2004 (American Institute of Aeronautics and Astronautics,Washington, DC, 2004), AIAA-2004-3777.
[18] E. Ahedo and F. I. Parra, Phys. Plasmas **12**, 073503 (2005).
[19] Y. Raitses, D. Staack, and N. Fisch, *Proceedings of the 38th Joint Propulsion Conference*, Indianapolis, IN, July 7–10, 2002 (American Institute of Aeronautics and Astronautics, Washington, DC, 2002), AIAA-2002-3954.